Supplemental Information

Supplemental Methods

Mice

The strategy used to construct the *Annex1*$^{-/-}$ mice has been previously described (1). To ensure that the knockout strategy used to construct the *Annex1*$^{-/-}$ mice did not affect other gene(s) being transcribed on the opposite strand or at the vicinity of *Anax1* we have carefully analyzed the genomic region where *Anax1* is located. Based on the latest assembly of the mouse genome (GRCm38/mm10) no gene is encoded by the reverse strand of the Anax1 coding gene. Moreover, Anax1 is very far away from any other coding genes: the two closest genes to Anax1 are the aldehyde dehydrogenase family 1, subfamily A1 (*Aldh1a1*) and *Aldh1a2* genes, which are located 211 kilobases and 302 kilobases away from the transcription start site of Anax1, respectively.

Histopathology and bacterial staining

Lung tissues were fixed in 10% formalin for H&E staining. Bacterial staining was performed with auramine/rhodamine (TB fluorescent stain kit T, BD Biosciences) or ziehl neelsen staining according to manufacturer's protocol.

Adoptive transfer

$CD3^+$ T cells were purified from spleens of naïve WT and *Annex1*$^{-/-}$ mice using MACS column purification procedure by negative selection (Pan T cell kit - MACS Miltylene). The purity was more than 95%. One million $CD3^+$ T cells were transferred intravenously to $Rag1^{-/-}$ recipient mice. One day later, $Rag1^{-/-}$ mice were infected via aerosol route with 50-100 H37Rv. $CD8^+$ T cells were purified from spleen and lymph nodes of OT-I mice (OT-I TCR-transgenic $CD8^+$ T cells) using MACS column purification procedure by negative selection ($CD8^+$ T cell kit - MACS Miltylene). The purity of $CD8^+$ T cells was usually between 92-97%. Purified $CD8^+$ T cells were stained with 5μM CFSE in PBS containing 0.1% BSA at room temperature. Staining was stopped after 8 min of incubation by addition of RPMI medium containing 10% FBS. $5x10^5$ cells were transferred intravenously (via retro-orbital vein) to WT and *Annex1*$^{-/-}$ mice. One day later, mice were infected in the footpad with 10^6 BCG-OVA in PBS containing 0.05% Tween 80.

Four days after infection, draining popliteal lymph nodes were harvested and cells were stained with H-2K^{b}-SIINFEKL tetramer APC and anti-CD8 PercP as described in the section flow cytometry. The percentage of SIINFEKL-specific CD8^{+} T cell was determined by tetramer positive cells (APC positive gate) inside CD8^{+} T cells (PercP positive gate) population. CD8^{+} T cell proliferation was measured by reduction in CFSE expression (CFSE^{low}) of OVA specific CD8^{+} T cell population.

Extraction of RNA and real-time PCR

For BMDC, RNA extraction was performed with TRIzol/chloroform (Invitrogen). RT was performed with iScript cDNA Synthesis Kit (Bio-Rad) and qPCR was performed with SsoFast Eva Green with low ROX (Bio-Rad) on an Mx3005 qPCR machine (Agilent). CD3^{+} T cells were purified from spleens and lymph nodes of T cells$^{Annex1+/+}$ and T cells$^{Annex1-/-}$ chimeric mice using MACS column purification procedure by negative selection (Pan T cell kit - MACS Miltylene). The purity of CD3^{+} T cells was 92%. RNA was extracted from purified CD3^{+} T cells by using the TRIzol reagent (Invitrogen) and processed for mRNA analysis by reverse transcriptase quantitative PCR (RT-QPCR). In brief, 500ng of total RNA was reverse transcribed in a total volume of 20μl by using Moloney murine leukemia virus reverse transcriptase (QuantiTec Reverse Transcription Kit, Qiagen. Raw Ct values were obtained from Bio-Rad CXT96 qPCR instrument. Results were analyzed using the formula $2^{-\Delta Ct}$ formula normalizing target gene expression to GAPDH. Primers used are listed in Supplemental Table 3.

Cell death analysis

BMDM were generated from WT and *Annex1*$^{-/-}$ mice as described above. Cells (10^5) were infected with H37Rv at the MOI of 5 and 10 for 4h at 37^{o}C. Cells were washed twice and kept at 37^{o}C, 5% CO_2, for 48h. After this period, apoptosis and necrosis was assessed by a commercially available cell death detection ELISAplus photometric enzyme immunoassay (Roche Applied Science) according to manufacturer's protocol. The amount of apoptosis was calculated as a ratio of the absorbance of infected macrophages to that of uninfected control macrophages. For infection with avirulent *Mtb* (H37Ra), 10^6 cells were infected at the MOI of 10 as described previously. Forty-eight hours after infection, cells were harvested, washed in cold PBS and

stained in binding buffer with 7AAD and anti-Annexin V antibody in the dark at room temperature. After 15 min, 400μl of binding buffer were added and cells were acquired within 1h.

Western blot

Western blotting was performed with proteins from whole extract of lysed apoptotic vesicles and from the membrane and cytosolic fractions. Apoptotic vesicles were lysed with RIPA buffer (1.5M NaCl, 0.5M EDTA, 10% deoxycholate, 10% SDS, 1M Tris-HCl pH7.4, Triton X100, protease inhibitor cocktail). Cell lysis extraction was centrifuged at 10000rpm for 10min to separate nuclear from cytosol/membrane fraction. Cytosol and membrane fractions were then separated by ultracentrifugation at 100000g for 2h at 4^{o}C. Sixty micrograms of proteins were loaded on SDS-10% polyacrylamide gels. Proteins were then transferred onto a nitrocellulose membrane, blocked with 5% milk, and probed with anti-annexin1 antibody (cell signaling), followed by treatment with anti-rabbit antibody conjugated to HRP. Blot was further developed using an ECL substrate (Bio-Rad), and bands were identified by enhanced chemiluminescence (Chemi-Doc, Bio-Rad).

Morphology and Electron Microscopy

Scanning electron microscopy (SEM) was employed to determine the three dimensional morphology of the obtained apoptotic vesicles. Samples were prepared by diluting the vesicle sample in 2.5% gluteraldehyde fixative (Sigma-Aldrich, Oakville, Ontario). The fixed sample was then allowed to adhere to poly-l-lysine coated 12mm cover glass, followed by an ethanol dehydration series of 30, 50, 70 and 100% ethanol. The sample was then gold-palladium sputtered using a Hummer VI Au-Pd Sputter Coater (Anatech Ltd., Arlington, Virginia). SEM imaging was then performed using a FEI Quanta 200 Environmental SEM System (FEI Company, Hillsboro, Oregon).

Vesicle Size and Surface Charge

Average hydrodynamic diameter (size) and size distribution (polydispersity index; PI) of WT and *Annex1*$^{-/-}$ vesicles were assessed at 25 °C by a particle sizer using a low-angle laser light-scattering device (HPPS, Malvern Instruments). The net surface charge was determined by zeta

(ζ) potential with a ZetaPlus analyzer using laser Doppler anemometry (Brookhaven Instruments, USA). Vesicle size was measured by flow cytometry. Using a side-scatter (SSC) threshold of 800 arbitrary units the lower sensitivity of the instrument was established and the SSC and forward scatter (FSC) voltages were set in log scale. Vesicle gates were determined using standard beads of various sizes (0.22μm, 0.45μm, 0.88μm and 1.34μm; Spherotec Inc, Lake Forest, IL). Both standard beads and apoptotic vesicles were diluted in 0.5% BSA/PBS and acquired on the low flow setting.

Gene Ontology (GO) and Pathway Enrichment Analysis.

We used GeneTrail (2) to test for enrichment of functional annotations among the 18 genes for which expression levels were significantly associated with the expression levels of *ANAX1* in human DCs. We used all expressed genes (i.e., 12,958 genes) as a background set. The tests were performed using all GO categories and Kyoto Encyclopedia of Genes and Genomes pathways. P values were calculated by comparing the observed data with the quantiles of a hypergeometric distribution, and we used the approach of Benjamini and Hochberg (3) to control the false discovery rate. To further evaluate the likelihood of finding four of 18 genes asscociated with endosome or lysome functions we generated 100,000 random sets of 18 genes taken for the 12,958 genes interrogated in our dataset. We then counted the number of genes in each random set that belonged to the gene ontology term ‘Endosome Membrane‘ (GO:0010008) or the KEGG pathways ‘lysosome’ (hsa04142). The resulting distribution was compared to the observed number in our data to generate an empirical *P*-value.

Supplemental References

1. Hannon R, Croxtall JD, Getting SJ, Roviezzo F, Yona S, Paul-Clark MJ, et al. Aberrant inflammation and resistance to glucocorticoids in annexin 1-/- mouse. FASEB J Off Publ Fed Am Soc Exp Biol. 2003 Feb;17(2):253–5.

2. Backes C, Keller A, Kuentzer J, Kneissl B, Comtesse N, Elnakady YA, et al. GeneTrail--advanced gene set enrichment analysis. *Nucleic Acids Res*. 2007;35(Web Server issue):W186–192.

3. Benjamini Y, Hochberg Y. Controlling the False Discovery Rate: A Practical and Powerful Approach to Multiple Testing. *J R Stat Soc Ser B Methodol*. 1995;57(1):289–300.

Supplemental Figure 1. WT and *Annex1-/-* mice present similar levels of total T cell response after aerosol infection with *M. tuberculosis*. (A-D) WT and *Annex1*$^{-/-}$ mice were infected with 50-100 CFU of virulent Mtb via aerosol route. (A) Histopathology of *Annex1*$^{-/-}$ mice prior to death revealed severe diffuse chronic active histiocytic pneumonitis with extensive replacement of air space with inflammatory cells and (B) increased number of *M. tuberculosis* (original maginification, X40 , X400, and for the bacteria X1000). The percentage of $CD4^+$ (C) and $CD8^+$ (D) T cells were evaluated by flow cytometry. Results are a pool of two independent experiments (n=4-5 mice per group). There was no significant difference between groups (*t*-test).

Supplemental Figure 2. Annexin1 is dispensable in T cells. (A) T cells were purified from spleens of WT and *Annex1*$^{-/-}$ mice. RNA was extracted from purified T cells and the expression of several members of annexin family or genes involved in eicosanoid pathways was evaluated by real time PCR. (B) Strategy of generating mixed bone chimeric mice whose T cells are lacking annexin1, but in any other myeloid compartment annexin1 is intact. (C-H) Chimeric mice were generated as described in material and methods. (C) After 12-weeks of reconstitution, T cells were purified (92% purity) from chimeric T cells$^{Annex1-/-}$ mice and chimeric T cells$^{Annex1+/+}$ mice. The absence (hashed grey bar – T cells) and presence (grey bar – T cells) of annexin1 respectively, was confirmed at RNA level. The tiny amount of annexin1 mRNA detected in T cells$^{Annex1-/-}$ was due to 8% of contamination by other non T cells. Cells isolated from non T cell compartment of both T cells$^{Annex1-/-}$ (hashed grey bar – non T cells compartment) and T cells$^{Annex1+/+}$ (grey bar – non T cells compartment) mice expressed high levels of annexin1. As a positive and negative control, we measured mRNA expression from purified T cells and other non T cells from WT (white bars) and *Annex1*$^{-/-}$ (hashed white bars), respectively. ND= non detected. (D-E) BMDC were generated from chimeric mice as described in materials and methods. $2.5x10^5$ cells were stimulated with 100ng/ml of LPS. Twenty four hours later, (D) phenotype of BMDC was determined by flow cytometry and (E) the amount of TNFα produced by BMDC was measured in the supernatant of the culture by ELISA. Numbers above bracketed lines (D) indicate the percentage of $CD11c^+$ (left) cells; percentage of $CD86^{high}$ (second from left to right), $CD80^{high}$ (third from left to right) and $CD40^{high}$ (right) on the $CD11c^+$ population. (F-G) Twelve weeks after reconstitution, chimeric mice were infected via aerosol route with 50-100 CFUs of H37Rv. (F) Percentage of $CD4^+$ and (G) $CD8^+$ T cells was evaluated by flow

cytometry. (H) Bacterial burden in the spleen after different time points of infection. There was no significant difference between both groups (*t*-test).

Supplemental Figure 3. Cell death modality of *Mtb* infected macrophages is not regulated by annexin 1. (A-B) BMDM were infected with H37Rv at the MOI of 5 and 10. After 48h, the levels of apoptosis (A) or necrosis (B) were evaluated by cell death ELISA kit. (C-E) BMDM were infected with H37Ra at the MOI of 5 and 10. After 48h, the levels of apoptosis (D) or necrosis (E) were evaluated by staining with Annexin V and 7AAD. There was no significant difference between groups (*t*-test).

Supplemental Figure 4. Characterization of apoptotic vesicles. WT and *Annex1*$^{-/-}$ apoptotic vesicles purified from supernatant of BCG-OVA infected WT and Annex1$^{-/-}$ BMDM. (A) Bacterial growth from WT and *Annex1*$^{-/-}$ BMDM after 4h and 4 days of BCG-OVA infection. (B) Scanning electron microscopy with scale bar of 500nm. (C) Membrane and cytosolic fractions of apoptotic vesicles were separated by ultracentrifugation at 100000g. Proteins were separated by SDS-PAGE, blotted to nitrocellulose, and stained with an annexin1 antibody. A band of ~37 KDa corresponding to the annexin1 fragment is demonstrated for both cytosolic and membrane fraction of WT vesicles in contrast to *Annex1*$^{-/-}$ apoptotic vesicles. (D) Standard beads of different sizes (0.22μm, 0.45μm, 0.88μm and 1.34μm) were used to determine the gating strategy. (E) Size resolution of WT (left) and *Annex1*$^{-/-}$ (right) vesicles based on beads gating strategy. (F) Average hydrodynamic diameter (size) and size distribution (polydispersity index; PI) of WT and *Annex1*$^{-/-}$ vesicles assessed at 25^{o}C by a particle sizer using a low angle laser light-scattering device. The net surface charge was determined by zeta (ζ) potential with a ZetaPlus analyzer using laser Doppler anemometry. (G) Expression of phosphatydilserine on the surface of apoptotic WT (left) and *Annex1*$^{-/-}$ (right) vesicles of different sizes (0.22μm – blue; 0.45μm – red; 0.88μm – purple and 1.34μm – green) detected by Annexin V staining. (H) Bone marrow derived DC^{WT} were loaded with PKH26-labeled WT or *Annex1*$^{-/-}$ vesicles. Quantification of cellular uptake based on the ratio of fluorescence intensity of uptaken vesicles (red) relative to cell nuclei (blue).

Supplemental Figure 5. Expression of annexin1 on apoptotic vesicles and cells regulates T cell

response. (A) CFSE-labeled WT or *Annex1*$^{-/-}$ apoptotic cells were injected (i.v.) into WT mice (n=3). One hour after injection of apoptotic cells, splenic DCs were enriched with positive selection and CD8^{+}DCs were gated from the CD11c^{+}MHC-II^{high} population. Numbers above outlined areas indicate the percentage of CD11c^{+}MHC-II^{high} cells. (B) PKH26-labeled WT or *Annex1*$^{-/-}$ apoptotic vesicles were injected (footpad) into WT mice (n=3). After 1h, localization of injected apoptotic vesicles were examined in the sections of popLN. The sections were stained with anti-CD11c or CD8 (green) and B220 (blue); Scale bars: 100 μm. The white squares are enlarged views showing the majority of PKH26-labeled apoptotic cells (red) were localized with either CD11c^{+} or CD8^{+} DCs in the interfollicular regions; Scale bars: 30 μm. (C) Bone marrow derived DC^{WT} loaded with 1mg/ml of WT or *Annex1*$^{-/-}$ vesicles were co-cultured with CFSE-labeled, purified OT-I CD8^{+} T cells. At day 3, CD8^{+} T cell proliferation was evaluated using CFSE dilution. Controls were CFSE-labeled OT-I TCR-transgenic CD8^{+} T cells cultured with DC^{WT} without vesicles. Numbers above outlined areas (C) indicate the percentage of CFSE^{low} cells. Results are representative of two independent experiments. * $p<0.05$ (*t*-test). (D) CFSE-labeled CD8^{+} T cells were adoptively transferred (i.v.) into WT mice (n=4). The following day, mice were injected with WT or *Annex1*$^{-/-}$ OVA-loaded apoptotic cells (i.v). (D) Frequency and total cell number of SIINFEKL-specific CD8+T cells from spleens at day 3 after injection of apoptotic cells. Numbers above gate indicate the percentage of CD8^{+} T cells stained with H-2K^{b}-SIINFEKL *, $p<0.05$ (*t*-test)

Supplemental Figure 6. Annexin1 does not regulate DC maturation or migration. (A) WT and *Annex1*$^{-/-}$ BMDC (DC^{WT} and DC$^{Annex1-/-}$) were loaded with 10^{-5}μM or 10^{-6}μM OVA peptide (SIINFEKL). After 4h, CFSE-labeled, purified OT-I TCR-transgenic CD8^{+} T cells were added to the culture. At day 2, CD8^{+} T cell proliferation was evaluated using CFSE dilution. Controls were CFSE-labeled purified OT-I TCR-transgenic CD8^{+} T cells cultured with BMDC without peptide. Results are a pool of two independent experiments. (B-D) CFSE-labeled WT apoptotic cells were injected (i.v.) into WT or *Annex1*$^{-/-}$ mice (n=3). One hour after injection of apoptotic cells, splenic DCs were enriched with positive selection and CD8^{+}DCs were gated from the CD11c^{+}MHC-II^{high} population. (E-F) WT and Annex1$^{-/-}$ mice were intranasal injected with 10μg of LPS. One day later, migration of DCs to lung draining lymph nodes was evaluated. Frequency (E) and total numbers (G) of DCs (CD11c^{+}MHCII^{high}); and frequency (F) and total numbers of

$CD103^{+}$DCs (H) and $CD11b^{+}$DCs (I) in the lung draining LN.(J-N) Bone marrow derived DC^{WT} and $DC^{Annex1-/-}$ were infected with BCG-OVA (MOI~10). (J) At different time points (4h, 6h and 24h), DC maturation was evaluated based on expression of CD40, CD80, MHC-II and MHC-I. Kinetics of Median fluorescence intensity for CD40 (K), CD80 (L), MHC-II (M) and MHC-I (N) expression on the surface of DC^{WT} and $DC^{Annex1-/-}$. Results are representative of two independent experiments. There was no significant difference between groups (*t*-test).

Supplemental Figure 7. Absence of annexin1 gene does not alter expression of other annexin family members or genes involved in the eicosanoide pathways. (A) WT or *Annex1*$^{-/-}$ BMDC were infected with BCG-OVA (MOI~10) for 4h. At different time points, supernatant of cell culture was collected and cells were harvested for RNA extraction. Expression of annexins 1, 2, 4, 6 and 10, NOS2, cPLA2, sPLA2, mPGES1, and 5LO were evaluated by real time PCR. (B) PGE2 and 5LO production by BCG-OVA infected BMDC was evaluated by ELISA.

Supplemental Figure 8. Correlation between *ANAX1* expression levels in *Mtb*-infected DCs and the expression levels of TBK-1 (TANK-binding kinase 1), CD68 (a member of the lysosomal/endosomal-associated membrane glycoprotein, LAMP), HEXB (Hexosaminidase B, which is the beta subunit of the lysosomal enzyme), and FAM125B (which encodes protein for the endosomal sorting complexes required for transport (ESCRT) machinery). These genes are all associated with the endosome/lysosome pathway.

Supplemental Table 1: Correlation levels between *ANXA1* expression levels in MTB-infected DCs and the expression levels of 12,957 other genes.

Supplemental Table 2. Gene Ontology and pathways enrichment analyses for the set of genes for which expression levels were found to be significantly associated with the expression levels of *ANXA1* in *Mtb*-infected DCs.

Supplemental Table 3. Sequence of the primers used for real time PCR in this study.

Supplemental Figure 1

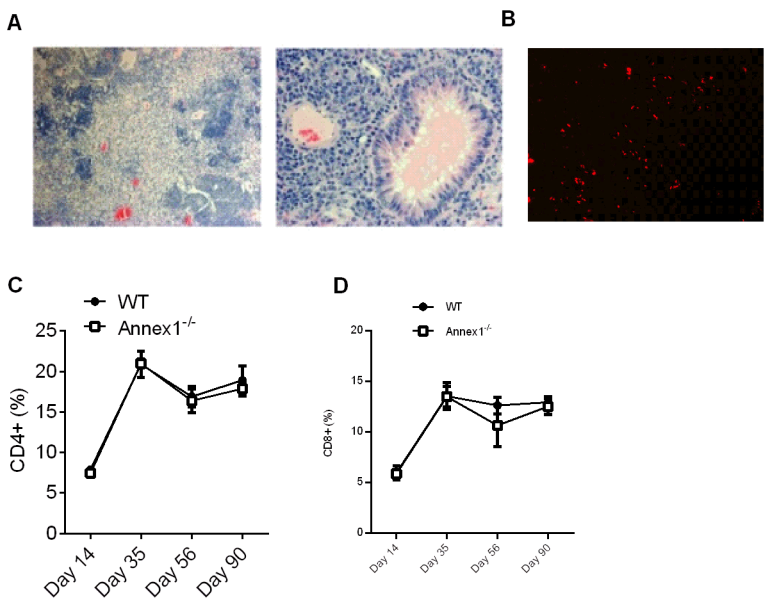

Supplemental Figure 2

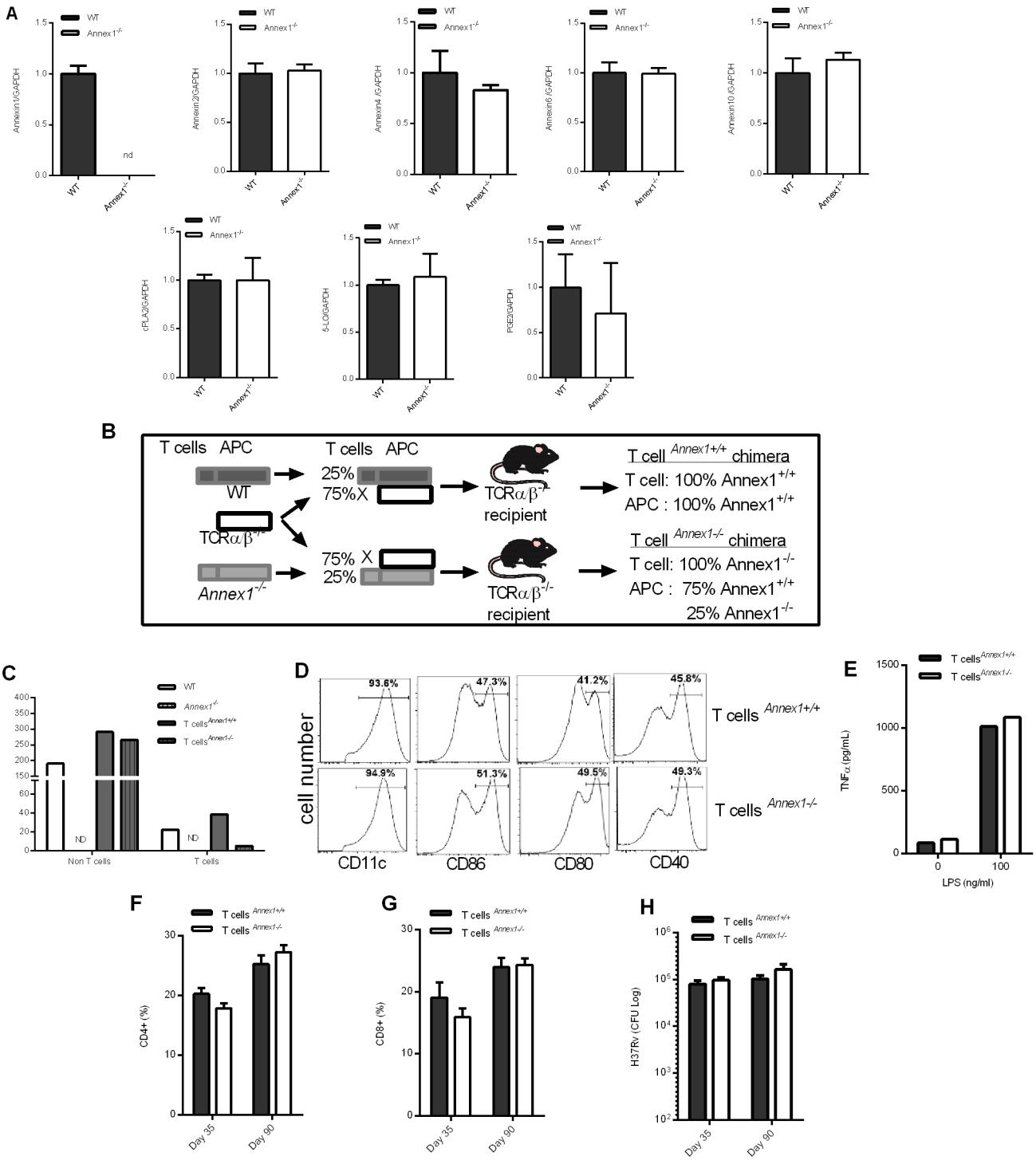

Supplemental Figure 3

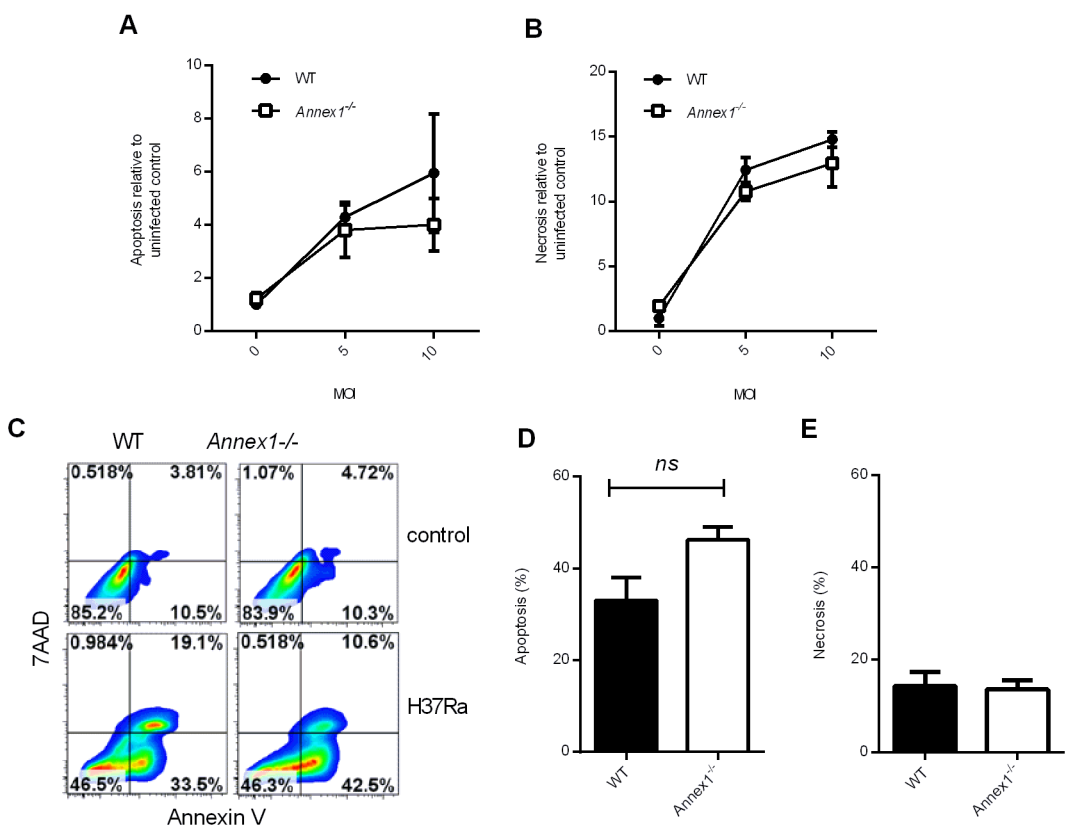

Supplemental Figure 4

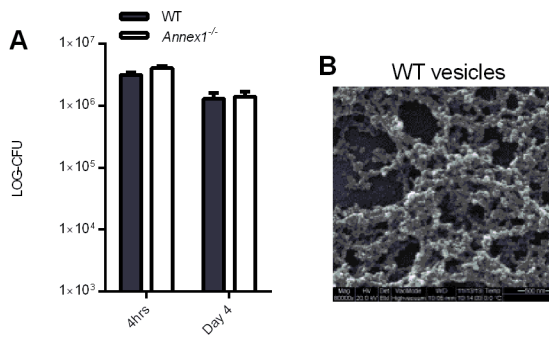

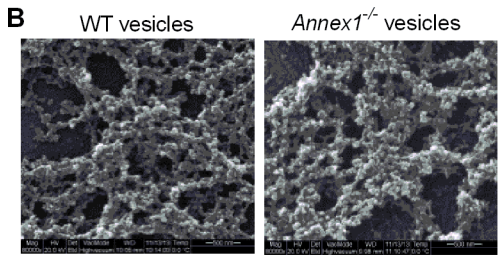

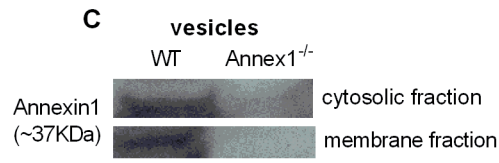

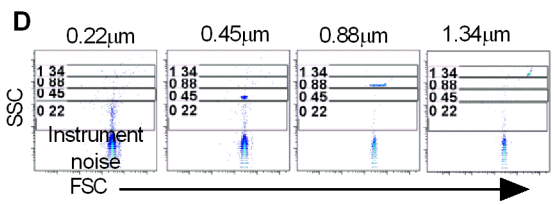

F

Vesicles	Size	Polydispersity	Zeta Potential	Std. Error
WT	126nm	0.362	-29.80mV	5.14mV
Annex1-/-	111.9nm	0.37	-34.87mV	4.27mV

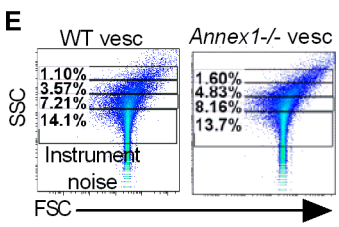

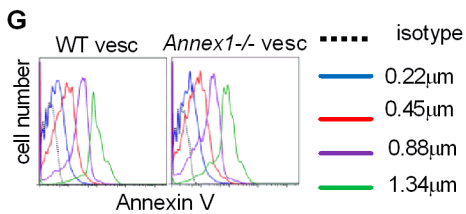

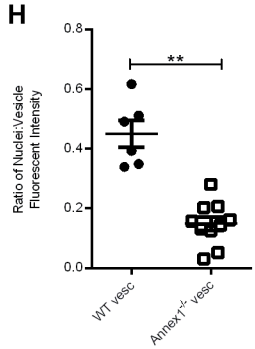

Supplemental Figure 5

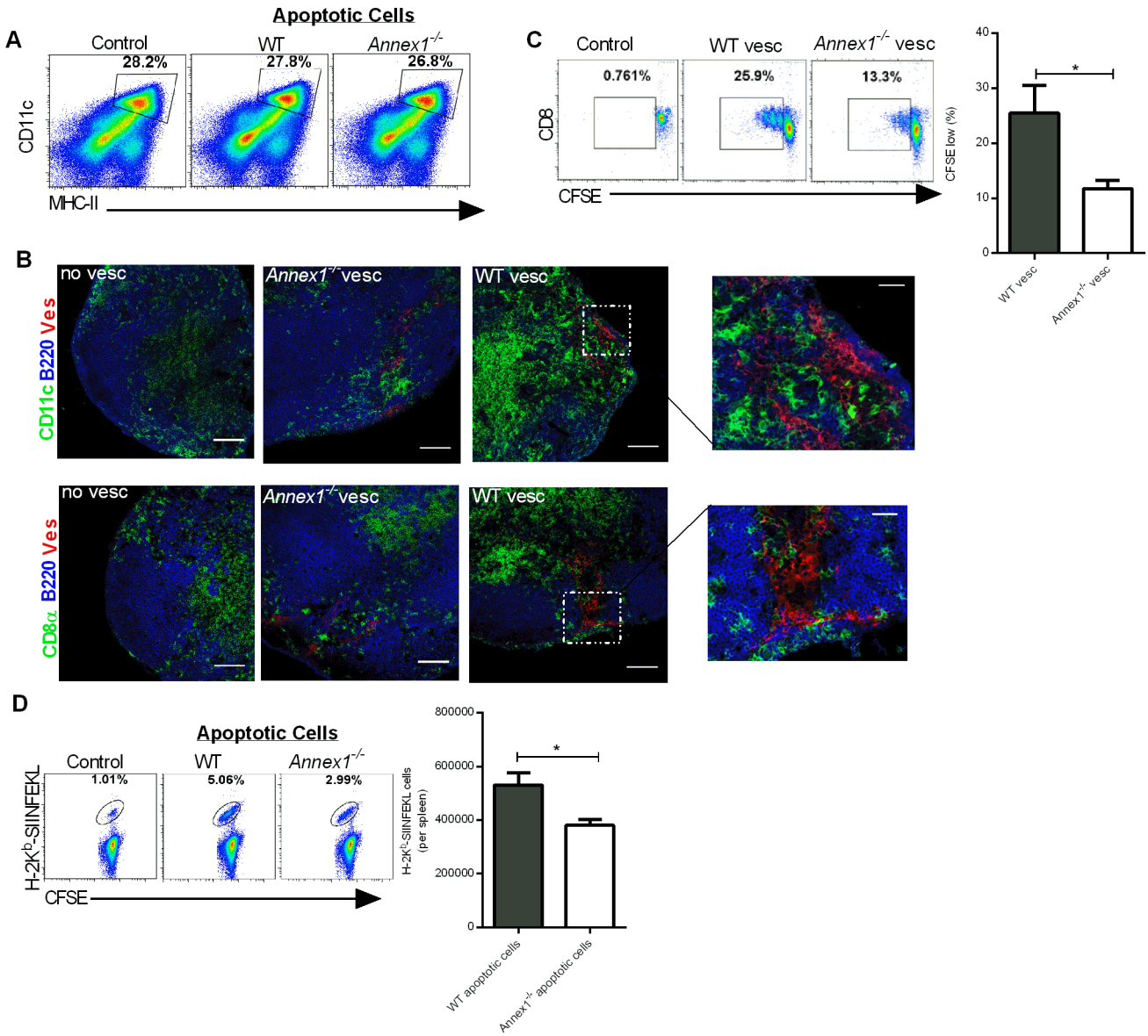

Supplemental Figure 6

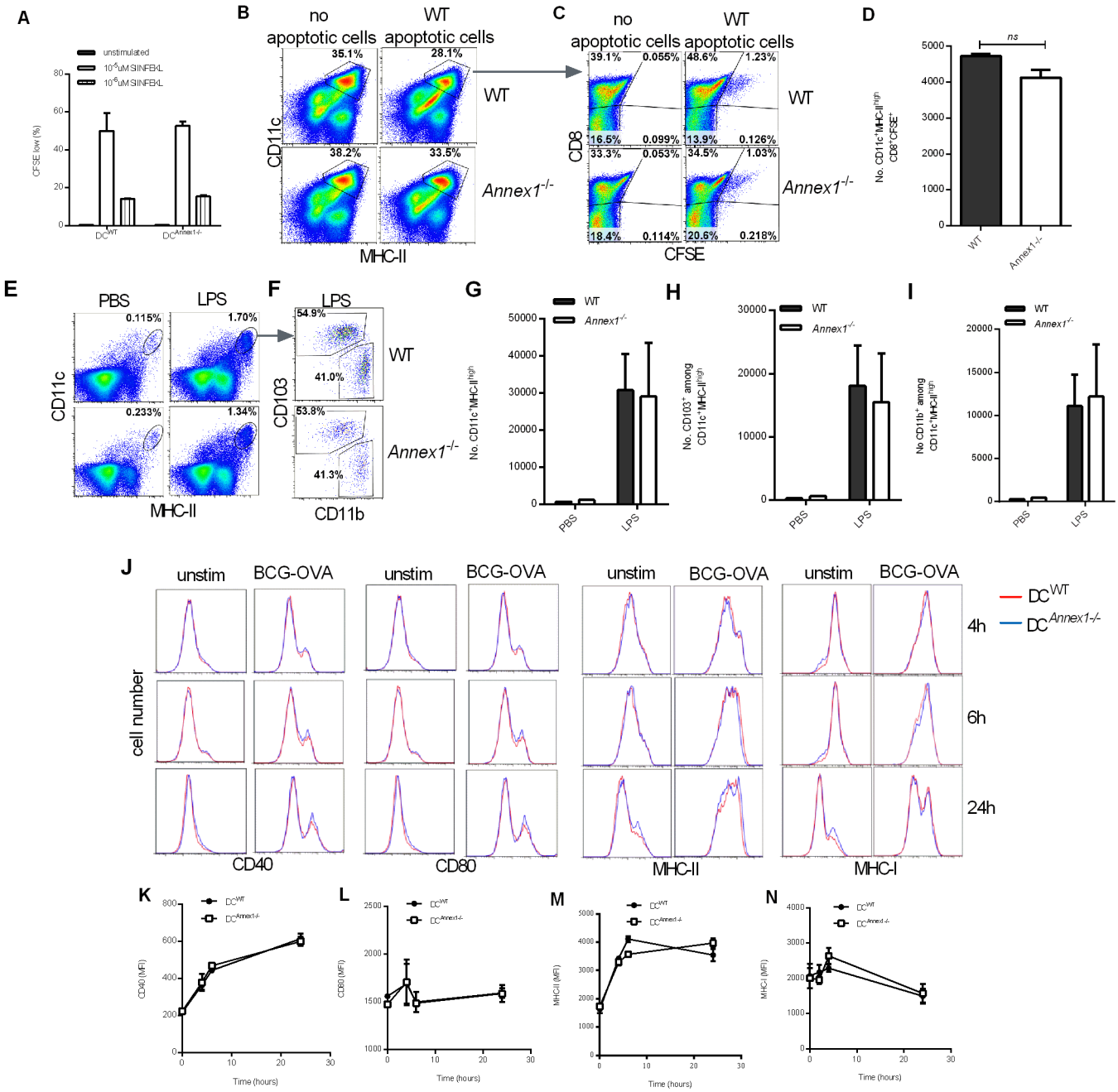

Supplemental Figure 7

A

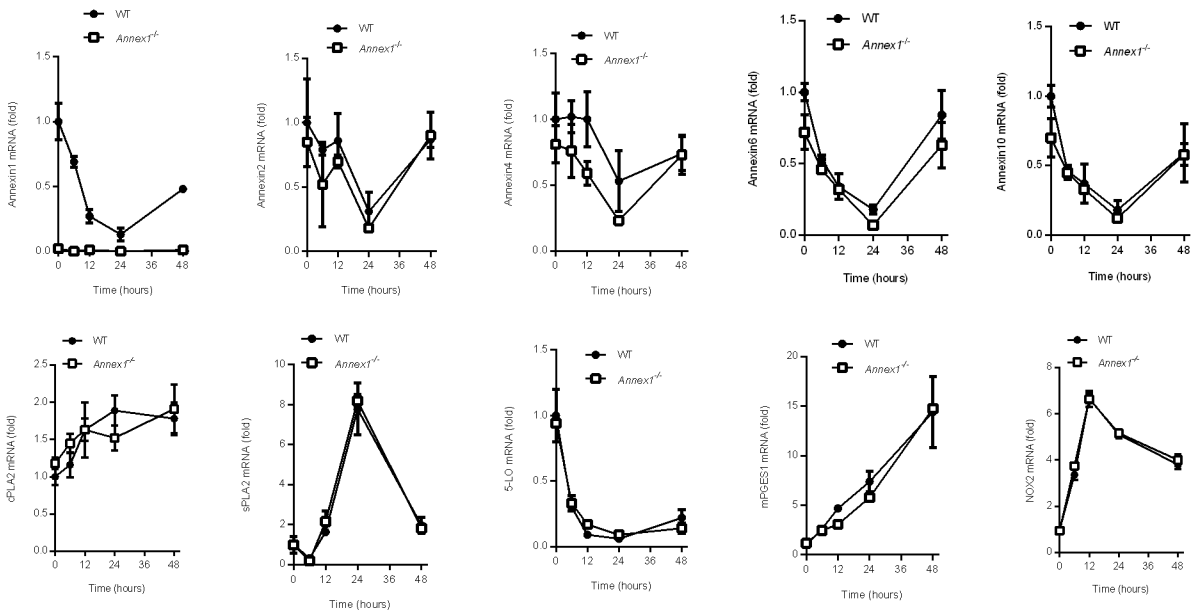

B

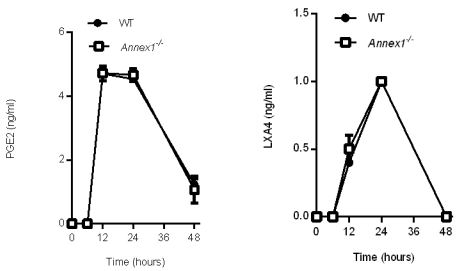

Supplementary Fig 8

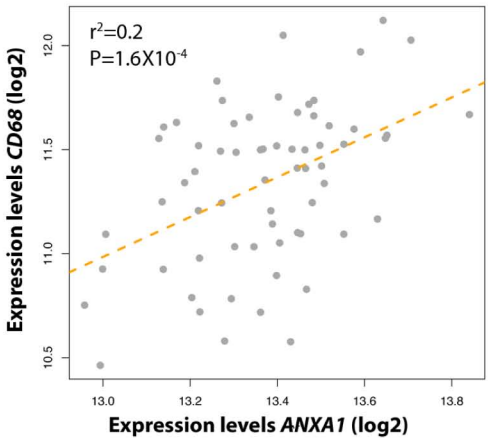

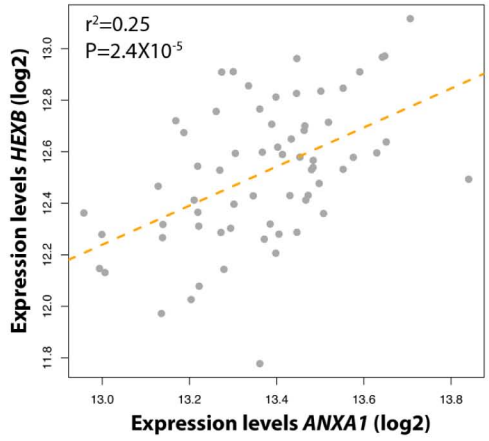

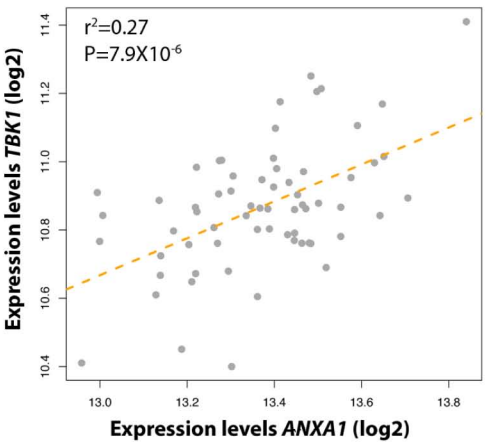

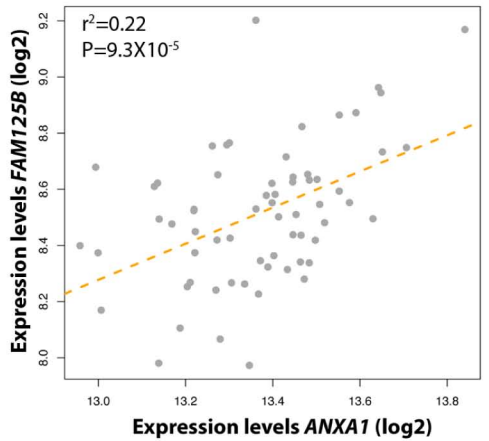

Table 3. List of primers

Gene (mouse)	Forward sequence (5'-3')	Reverse sequence (5'-3')
Annexin1	CCCTACCCTTCCTTCAATGTATC	AGCATTGGTCCTCTTGGTAAG
Annexin2	AAGGGAGGCTCTCAGCGATA	TTTGACTGACCCGTAGGCAC
Annexin4	TTCTCCGCACCAGAGGAACT	TGGGCATCTTCAGTTGCGTT
Annexin6	ATCACAAGTCCCTGGAGGATG	GTGTCTGCTATTTCCTGGGCA
Annexin10	AGCTGGGACCTATCAGAGCA	TGGAGGATACATCAGGCCCA
mPGES1	CACAGAGCAAAGCACTGTCCA	TCGAGAGATGCAAGAGATGCT
5LO	GGAACTGCAGGACTTCGTGA	CGTGAAGATCACCACCGTCA
cPLA2	AAGTCGGAACTGTGAAGGGC	CATTTTGGTCCCAGTTGCAGA
sPLA2	ATGTTTCGCCCGGAACAAGA	CATGTCCGGGTGTTTCAGGA
NOS2	TTCACTCCACGGAGTAGCCT	AGAGAAACTTCCAGGGGCAAG
GAPDH	GCGTCGTGATTAGCGATGATG	CTCGAGCAAGTCTTTCAGTCC